Published in final edited form as:
*Biomed Signal Process Control*. 2012 September 1; 7(5): 438–446. doi:10.1016/j.bspc.2011.11.005.

# A study of non-invasive Patlak quantification for whole-body dynamic FDG-PET studies of mice

**Xiujuan Zheng**[a,b,*], **Lingfeng Wen**[c,d], **Shu-Jung Yu**[e], **Sung-Cheng Huang**[e], and **David Dagan Feng**[b,c]

[a]School of Medicine, Shanghai Jiaotong University, Shanghai, China

[b]Department of Electronic and Information Engineering, Hong Kong Polytechnic University, Hong Kong

[c]School of Information Technologies, The University of Sydney, Sydney, Australia

[d]Department of PET and Nuclear Medicine, Royal Prince Alfred Hospital, Sydney, Australia

[e]Department of Molecular and Medical Pharmacology, David Geffen School of Medicine at UCLA, University of California, Los Angeles, CA, USA

## Abstract

Physiological changes in dynamic PET images can be quantitatively estimated by kinetic modeling technique. The process of PET quantification usually requires an input function in the form of a plasma-time activity curve (PTAC), which is generally obtained by invasive arterial blood sampling. However, invasive arterial blood sampling poses many challenges especially for small animal studies, due to the subjects' limited blood volume and small blood vessels. A simple non-invasive quantification method based on Patlak graphical analysis (PGA) has been recently proposed to use a reference region to derive the relative influx rate for a target region without invasive blood sampling, and evaluated by using the simulation data of human brain FDG-PET studies. In this study, the non-invasive Patlak (nPGA) method was extended to whole-body dynamic small animal FDG-PET studies. The performance of nPGA was systematically investigated by using experimental mouse studies and computer simulations. The mouse studies showed high linearity of relative influx rates between the nPGA and PGA for most pairs of reference and target regions, when an appropriate underlying kinetic model was used. The simulation results demonstrated that the accuracy of the nPGA method was comparable to that of the PGA method, with a higher reliability for most pairs of reference and target regions. The results proved that the nPGA method could provide a non-invasive and indirect way for quantifying the FDG kinetics of tumor in small animal studies.

### Keywords

Non-invasive; Patlak graphical analysis; Parameter estimation; FDG-PET

## 1. Introduction

Positron emission tomography (PET) is a popular functional imaging technology that visualizes physiological changes through the administration of radiopharmaceutical molecular tracers into living systems. $^{18}$F-fluorodeoxyglucose (FDG) is the most widely



*Corresponding author at: School of Medicine, Shanghai Jiaotong University, Shanghai, China. zhengxj@shsmu.edu.cn (X. Zheng).

used tracer in PET studies, and it is mainly used for the in vivo measurement of glucose metabolism. The visualization of subtle metabolic changes is especially attractive for the early detection of malignant tumors, which usually have elevated glucose metabolism. Thus PET imaging with FDG (FDG-PET) has become an important tool in clinical oncology for cancer diagnosis, staging, treatment planning and response assessment [1]. One unique benefit of functional imaging is that quantitative functional parameters can be derived by using tracer kinetic modeling techniques. This delivers a simple way for the quantitative description and objective comparison of complex physiological processes. The process of parameter estimation for deriving physiological parameters is usually based on an underlying kinetic model, which is specific to the used tracer. A plasma time–activity curve (PTAC) is usually used as an input function for a given kinetic model while a tissue time–activity curve (TTAC) derived from the dynamic PET images is used as an output function [2,3].

There are a number of different approaches for estimating the parameters of a kinetic model. The nonlinear least squares (NLS) method can provide statistically optimal estimates of the kinetic parameters through iteratively adjusting estimated parameters nonlinearly to achieve the minimum least squares difference between the measured and estimated TTACs [2]. Usually a weighted NLS method, referred to as WNLS, is used to address the comparable low signal to noise ratio in the early frames with shorter imaging durations. However, the NLS/WNLS methods with iterative processes have two drawbacks: the outcomes are highly sensitive to the choice of appropriate initial parameters, and the computation cost is high due to the slow converging speed [2]. The graphical analysis method was introduced to transform the nonlinear iterative parameter estimation process to a computationally efficient linear plot, whose slope or intercept reflects the parameters of interest [4,5]. For example, the slope of the Patlak graphical analysis (PGA) is equal to the influx rate, which is directly proportional to metabolic rate of glucose (MRGlc) in a FDG-PET study [4].

The process of obtaining a PTAC generally relies on frequent invasive arterial blood sampling. This process is relatively inconvenient and may expose operators to extra radiation. In particular, such invasive approaches are much more challenging for small animal studies because of the subjects' limited blood volume and small blood vessels. The image-derived methods [6–9] and population-based methods [10,11] have been presented to reduce or eliminate invasive blood sampling in kinetic modeling. Given multiple regions of interest (ROIs) with distinct TTACs, complex biological systems can be modeled as a single-input-multi-output (SIMO) system. The kinetic parameters and the input function can be estimated simultaneously when multiple distinct TTACs are available for different ROIs [12]. If a reference region is available to reflect the non-specific binding in a neuroreceptor study, the non-invasive Logan method can be used to avoid the problems associated with the traditional invasive Logan approach [13]. The slope of the linear regression of the non-invasive Logan method represents the ratio of the distribution volume between the target and the reference regions. Thus, it is potential for the Patlak method to be extended to derive the non-invasive estimation of the influx rate in FDG-PET studies with an appropriate reference region.

A non-invasive PGA (nPGA) method has been recently introduced for deriving a set of relative influx rates for FDG-PET studies by using reference regions. The method was evaluated using the simulated TTACs of different regions in the human brain [14]. However, it is unclear whether the nPGA method could be extended to whole-body small animal studies for multiple organs and regions. In this study, we aimed to systematically investigate the performance of the nPGA method in the quantification of glucose metabolism for small animal studies as compared with the traditional PGA method. The experimental FDG-PET studies of fifteen mice and computer simulations were used in the evaluation.

## 2. Theory

### 2.1. FDG Kinetic Modeling

The three-compartment four-parameter model shown in Fig. 1 is a general FDG kinetic model [2]. A parameter (vascular volume) representing the vascular effect is usually included to address spillover effect between tissues and the surrounding vascular system [11]. In this study, this three-compartment four-parameter model with vascular volume (3c4pVb) is referred as the general FDG model for differentiating from other kinds of the kinetic models.

The dynamic behavior of the tracer in tissue can be described in (1).

$$C_t(t)=(C_e(t)+C_m(t))+V_bC_p(t)=(B_1\exp(-L_1t)+B_2\exp(-L_2t))\otimes C_p(t)+V_bC_p(t) \quad (1)$$

where $C_p(t)$ (Bq ml$^{-1}$) and $C_t(t)$ (Bq ml$^{-1}$) denote the PTAC and TTAC, respectively; $C_e(t)$ (Bq ml$^{-1}$) is the concentration of FDG in tissue; $C_m(t)$ (Bq ml$^{-1}$) is the concentration of phosphorated FDG (FDG-6-PO$_4$) in tissue; $V_b$ (ml ml$^{-1}$) denotes vascular volume; and $L_1$, $L_2$, $B_1$ and $B_2$ are macro parameters that are the combination of rate constants as expressed in (2).

$$\begin{aligned} L_{1,2}&=\frac{k_2+k_3+k_4\mp\sqrt{(k_2+k_3+k_4)^2-4k_2k_4}}{2}\\ B_1&=\frac{K_1(k_3+k_4-L_1)}{L_2-L_1}\\ B_2&=\frac{K_1(L_2-k_3-k_4)}{L_2-L_1} \end{aligned} \quad (2)$$

The rate constants of $K_1$ (ml min$^{-1}$ ml$^{-1}$), $k_2$ (min$^{-1}$), $k_3$ (min$^{-1}$), $k_4$ (min$^{-1}$) and $V_b$ can be derived by parameter estimation. The MRGlc of the tissue can then be calculated according to (3):

$$\text{MRGlc}=K_i\frac{C_{glc}}{LC} \quad (3)$$

where $C_{glc}$ is the plasma glucose concentration; $LC$ is the lumped constant accounting for the differences in the transport and phosphorylation between FDG and glucose, and $K_i$ is the influx rate, as shown in (4).

$$K_i=\frac{K_1k_2}{k_2+k_3} \quad (4)$$

### 2.2. Patlak graphical analysis

Patlak graphical analysis (PGA) is a graphical analysis technique that is based on the assumption that $k_4$ in the general FDG kinetic model (Fig. 1) can be ignored [4]. The simple relationship between a PTAC and a TTAC can be given in (5):

$$\frac{C_t(t)}{C_p(t)}=K_i\frac{\int_0^t C_p(\tau)d\tau}{C_p(t)}+I,\ t>t^* \quad (5)$$

where the slope is equal to the influx rate $K_i$; the intercept $I$ is a constant; and $t^*$ is a sufficiently long time by which point an equilibrium has been reached between the FDG concentrations in plasma and in tissue. Thus, an estimate of $K_i$ can be derived from the slope of the linear plot of $\int_0^t C_p(\tau)d\tau/C_p(\tau)$ vs. $C_t(t)/C_p(t)$.

### 2.3. Non-invasive PGA

The nPGA method was proposed for deriving a relative influx rate using a reference region in the quantification of MRGlc for human brain FDG-PET studies [14]. It can be assumed that different ROIs have the same input function. The PGA equations for two distinct ROIs (one being the reference, the other being the target) are described in (6):

$$\begin{cases} C_{ref}(t)=K_{ref}\int_0^t C_p(\tau)d\tau+I_{ref}C_p(t) \\ C_{tg}(t)=K_{tg}\int_0^t C_p(\tau)d\tau+I_{tg}C_p(t) \end{cases}, t>t^* \quad (6)$$

where $C_{ref}(t)$ is the TTAC of the reference ROI, and $C_{tg}(t)$ is the TTAC of the target ROI.

Combining the Eqs. (6) into (7) eliminates the contribution of the PTAC and derives the relative influx rate, i.e. the ratio of influx rates between the target and reference regions. The relative influx rate can also be referred to as the target to reference relative influx rate. See the Appendix for more details on the derivation of (7).

$$\int_{t_0}^t C_{tg}(\tau)d\tau=K_{tr}\int_{t_0}^t C_{ref}(\tau)d\tau+I_{tr}[C_{ref}(t)-C_{ref}(t_0)]-I_{rr}[C_{tg}(t)-C_{tg}(t_0)], t>t_0>t^* \quad (7)$$

where $t_0$ is the mid-scan time of the first imaging frame, which is later than $t^*$, and $K_{tr}$ is the target to reference relative influx rate.

For the mid-scan time of the TTAC, where $t_0, t_1, t_2, \ldots, t_n > t^*$, (7) can be expressed in matrix form as given in (8):

$$y=X\theta_r+\varepsilon \quad (8)$$

where

$$y=\begin{bmatrix} \int_{t_0}^{t_1} C_{tg}(\tau)d\tau \\ \int_{t_0}^{t_2} C_{tg}(\tau)d\tau \\ \vdots \\ \int_{t_0}^{t_n} C_{tg}(\tau)d\tau \end{bmatrix}, X=\begin{bmatrix} \int_{t_0}^{t_1} C_{ref}(\tau)d\tau & C_{ref}(t_1)-C_{ref}(t_0) & -C_{tg}(t_1)+C_{tg}(t_0) \\ \int_{t_0}^{t_2} C_{ref}(\tau)d\tau & C_{ref}(t_2)-C_{ref}(t_0) & -C_{tg}(t_2)+C_{tg}(t_0) \\ \vdots & \vdots & \vdots \\ \int_{t_0}^{t_n} C_{ref}(\tau)d\tau & C_{ref}(t_n)-C_{ref}(t_0) & -C_{tg}(t_n)+C_{tg}(t_0) \end{bmatrix}, \theta_r=\begin{bmatrix} K_{tr} \\ I_{tr} \\ I_{rr} \end{bmatrix}, \text{and } \varepsilon=\begin{bmatrix} \varepsilon_1 \\ \varepsilon_2 \\ \vdots \\ \varepsilon_n \end{bmatrix}$$

. ε denotes the equation error term.

The target to reference relative influx rate can be solved using the linear least squares method as given in (9).

$$\hat{\theta}_r=(X^TX)^{-1}X^Ty \quad (9)$$

## 3. Methods

### 3.1. Small animal studies

Fifteen C57BL/6 mice (~27 g, non-fasting) were anesthetized with ~2% isoflurane and administered with FDG (~13 MBq, tail vein bolus). Five of these mice had been implanted with MCak tumors in both shoulders about one week prior to the FDG-PET studies. After FDG was administered, a 60-min dynamic imaging study was performed for each mouse on

a Focus 220 microPET scanner followed by a CT scan on a MicroCAT II scanner. Seven of these FDG-PET studies were conducted with a 31-frame imaging protocol: 15 × 0.5 s, 1 × 2 s, 1 × 4 s, 1 × 6 s, 1 × 15 s, 3 × 30 s, 1 × 60 s, 1 × 120 s, 3 × 80 s, and 4 × 900 s frames. The other eight FDG-PET studies were conducted with a 26-frame imaging protocol: 1 × 1.2 s, 10 × 0.4 s, 1 × 1.7 s, 2 × 5 s, 1 × 17.5 s, 1 × 45 s, 1 × 60 s, 1 × 90 s, 1 × 150 s, 1 × 180 s, 1 × 220 s, 1 × 365 s, and 4 × 550 s frames. The microCT image was aligned to the microPET images. 2D filtered back-projection with CT-based attenuation correction was applied to reconstruct PET images. Each frame was reconstructed with an image resolution of 128 × 128 × 95 voxels and a voxel size of 0.4 mm× 0.4 mm × 0.796 mm.

Sixteen blood samples were manually taken from a femoral catheter during the dynamic PET scan. Eq. (10) was used to derive the PTACs, as a means of obtaining the plasma activity from the blood samples [15]:

$$\begin{cases} C_p(t)=C_b(t) \times R_{FDG}(t) \\ R_{FDG}(t)=0.386e^{-0.191t}+1.165 \end{cases} \tag{10}$$

where $t$ is the blood sampling time in minutes after FDG injection, $C_p(t)$ is the PTAC, $C_b(t)$ is the FDG concentration in whole-blood samples, and $R_{FDG}(t)$ is a ratio function of plasma to whole blood.

Using the AMIDE software [16], ellipsoidal ROIs were manually delineated around the major organs on the reconstructed microPET images, with the aligned CT images acting as a guide. Due to the comparably small volumes of mice, the ROIs were delineated to cover entire organs. The tumor ROIs were also defined for the five tumor-bearing mice. The TTAC was derived by averaging the values of all the voxels within the ROI.

### 3.2. Computer simulations

The PTAC, $C_p(t)$, was simulated based on a mathematical model with 4 exponential components, as given by (11):

$$C_p(t)=A_1e^{\lambda_1 t}+A_2e^{\lambda_2 t}+A_3e^{\lambda_3 t}-(A_1+A_2+A_3)e^{\lambda_4 t} \tag{11}$$

where $A_1$ = 63.01 MBq ml$^{-1}$, $A_2$ = 4.95 MBq ml$^{-1}$, $A_3$ = 1.105 MBq ml$^{-1}$, $\lambda_1$ = 9.27 min$^{-1}$, $\lambda_2$ = 0.178 min$^{-1}$, $\lambda_3$ = 0.0157 min$^{-1}$, and $\lambda_4$ = 41 min$^{-1}$. These parameters were assigned according to the mean values given by Ferl et al. [9]. An 18-point blood sampling protocol was used with time points at 0.07, 0.11, 0.14, 0.17, 0.21, 0.24, 0.27, 0.31, 0.59, 0.9, 1.5, 4.5, 9.5, 15.5, 24.5, 34.5, 45.5 and 58.5 min post-injection.

A 26-frame 60-min imaging protocol was used in the simulation with 1 × 1.2 s, 10 × 0.4 s, 1 × 1.7 s, 2 × 5 s, 1 × 17.5 s, 1 × 45 s, 1 × 60 s, 1 × 90 s, 1 × 150 s, 1 × 180 s, 1 × 220 s, 1 × 365 s, and 4 × 550 s frames. The TTAC was then simulated based on (1), with the Gaussian noise $\varepsilon(t)$ added, as shown in (12):

$$\bar{C}_t(t)=C_t(t)+\varepsilon(t)=(B_1\exp(-L_1t)+B_2\exp(-L_2t))\otimes C_p(t)+V_bC_p(t)+\varepsilon(t) \tag{12}$$

where $\bar{C}_t(t)$ is the measurement of the TTAC; and the macro parameters, $B_1$, $B_2$, $L_1$ and $L_2$, are obtained from the combinations (shown in (2)) of the mean rate constants of certain organs derived from the fifteen FDG-PET studies of mice as shown in Table 1. $\varepsilon(t)$ is the PET measurement noise, which is assumed to be an additive, independent Gaussian noise with zero mean and variance as expressed in (13) [17,18]:

$$\sigma^2 = \frac{c \times e^{\lambda t} \times C_t(t)}{\Delta t} \tag{13}$$

where $c$ is a proportional constant determining noise level; $\lambda = \ln(2)/T_{1/2}$, $T_{1/2}$ is the half-life time of Fluorine-18 ($^{18}$F); and $\Delta t$ is the duration of imaging frame.

In this investigation, the values of $c$ were set to 0.1, 0.5, 1, 2 and 4, corresponding to noise levels ranging from 0.7% to 3% at the last measurement of the TTAC. One hundred TTACs were simulated at each noise level. One noise free TTAC was also simulated for the comparison.

### 3.3. Performance evaluation

The target to reference relative influx rate is defined as the ratio of the influx rate between the target and reference ROIs, as shown in (14):

$$K_{tr} = \frac{K_t}{K_r} \tag{14}$$

where $t$ is the index number of the target ROI, and $r$ is the index number of reference ROI. In this paper, the target index number $t$ was chosen to be 1, 2, 3, 4 or 5 for the brain, lungs, liver, muscle or tumor, respectively. The maximum index number for the reference ROI was 4. The tumor ROI was not used as a reference ROI.

In the small animal studies, the WNLS method has been applied to derive estimates of rate constants of the general FDG model by using the kinetic imaging system (KIS) [19]. The weights in the WNLS method were chosen to be proportional to the ratio between the imaging duration and the measurement in each frame [2,9]. The influx rates for each ROI were calculated according to (4), and then used to derive the relative influx rate between the target and reference ROIs according to (14). These relative influx rates were referred to as $K_{\text{tr,WNLS}}$. The mean rate constants obtained for each ROI in small animal studies were also used to derive the true value of the relative influx rate, referred to as $K_{\text{tr,true}}$, for the computer simulations.

The aforementioned PGA and nPGA methods were both used to derive the relative influx rates for the comparison. In particular, TTACs in the range of 3–22 min were used in PGA to estimate the influx rate for each ROI in order to minimize the influence of $k_4$ [15], allowing the derivation of the relative influx rate, $K_{\text{tr,PGA}}$. For the nPGA method, the relative influx rates were directly obtained by using the TTACs of the reference and target ROIs (excluded first 3-min data) according to (9). The relative influx rate as calculated by nPGA was referred to as $K_{\text{tr,nPGA}}$.

In the small animal studies, for each pair of target and reference ROIs, the mean and standard deviation (SD) of $K_{\text{tr,WNLS}}$, $K_{\text{tr,PGA}}$ and $K_{\text{tr,nPGA}}$ were calculated across the fifteen mouse studies. Moreover, linear regression analysis between $K_{\text{tr,WNLS}}$ and $K_{\text{tr,nPGA}}$ was applied to evaluate the performance of the nPGA method. The linear relationship between $K_{\text{tr,PGA}}$ and $K_{\text{tr,nPGA}}$ was also calculated.

In the computer simulations, the mean and SD values of $K_{\text{tr,PGA}}$ and $K_{\text{tr,nPGA}}$ were derived across the simulation data at same noise level. The coefficients of variation (CV) were derived according to the equation: (SD/mean) × 100%. Percentage bias of $K_{\text{tr,PGA}}$ and $K_{\text{tr,nPGA}}$ were derived by comparing the estimates with $K_{\text{tr,true}}$, according to ($|K_{tr} - K_{\text{tr,true}}|/K_{\text{tr,true}}$) × 100%.

### 3.4. Kinetic model investigation

Beside the general FDG model (3c4pVb), the three-compartment four-parameter model without vascular volume (3c4p), the three-compartment three-parameter model ($k_4 = 0$) with vascular volume (3c3pVb), and the three-compartment three-parameter model ($k_4 = 0$) without vascular volume (3c3p) could be used to analyze the FDG kinetics in brain and lung. It has been reported that the FDG kinetics in the skeletal muscles can be described by a four-compartment five-parameter model (5K model) [20].

Thus, the Akaike Information Criteria (AIC) and Schwarz Criteria (SC) [21] were used to evaluate the best kinetic model in characterizing FDG kinetics for the multiple regions in mouse studies. Theses kinetic models were then further used in investigating the effect of different kinetic models on the estimated biases of nPGA in computer simulations. The rate constants were directly estimated by WNLS with the four kinetic models: 3c3p, 3c3pVb, 3c4p, and 3c4pVb model. The percentage biases of $K_{tr}$ estimated by PGA and nPGA were calculated according to the reference relative influx rate obtained by WNLS respectively for each studied kinetic model.

## 4. Results

### 4.1. Rate constants of small animal studies

The rate constants of the general FDG model were estimated by using WNLS across fifteen FDG-PET studies of mice. Table 1 lists the mean and SD values of the estimated rate constants respectively for the brain, lung, liver, muscle and tumor. The obtained mean rate constants were then directly applied in computer simulations to generate simulated TTACs with various levels of noise added.

### 4.2. Relative influx rates in small animal studies

Table 2 lists the relative influx rate derived by the three methods: WNLS method ($K_{\text{tr,WNLS}}$), PGA method ($K_{\text{tr,PGA}}$) and nPGA method ($K_{\text{tr,nPGA}}$). Comparably similar relative influx rates were obtained by $K_{\text{tr,WNLS}}$, $K_{\text{tr,nPGA}}$ and $K_{\text{tr,PGA}}$ for the targets of lung, muscle and tumor, when the brain was chosen as the reference ROI. Similar results were observed when the lung ROI was used as the reference. When the muscle was chosen as the reference ROI, similar result was also observed between $K_{\text{tr,nPGA}}$ and $K_{\text{tr,PGA}}$ for the brain, lung and tumor as the target ROI. However, both $K_{\text{tr,nPGA}}$ and $K_{\text{tr,PGA}}$ were underestimated compared to $K_{\text{tr,WNLS}}$. The results were quite different when the liver was chosen as the reference ROI. Compared to $K_{\text{tr,WNLS}}$, $K_{\text{tr,PGA}}$ was overestimated while $K_{\text{tr,nPGA}}$ was underestimated. Fig. 2 shows the Bland–Altman plots for evaluating the agreement between $K_{\text{tr,nPGA}}$ and $K_{\text{tr,WNLS}}$ (Fig. 2A) and between $K_{\text{tr,nPGA}}$ and $K_{\text{tr,PGA}}$ (Fig. 2B) with the liver-related $K_{tr}$ excluded. The percentage difference between $K_{\text{tr,nPGA}}$ and $K_{\text{tr,WNLS}}$ in Fig. 2A was observed to be varied from −67% to 69%, while the mean difference was about 1.1%. Most (>90%) of all percent differences are within in a 69% range above/below the mean. In Fig. 2B, the mean of the percent difference between $K_{\text{tr,nPGA}}$ and $K_{\text{tr,PGA}}$ against their average was about −1.7%, and the limit of agreement was −55% to 51%. Most (>95%) of all percent differences are within in a 54% range above/below the mean.

Table 3 lists the linear regression analysis respectively for $K_{\text{tr,nPGA}}$ vs. $K_{\text{tr,WNLS}}$ and $K_{\text{tr,nPGA}}$ vs. $K_{\text{tr,PGA}}$ for the same reference groups. High linear correlations ($R^2 > 0.9$) were achieved for both $K_{\text{tr,nPGA}}$ vs. $K_{\text{tr,WNLS}}$ and $K_{\text{tr,nPGA}}$ vs. $K_{\text{tr,PGA}}$ except for the case where the liver was used as the reference; in this case a considerably lower linear correlation was achieved.

Table 4 lists the results of linear regression analysis of the estimates of $K_{tr,nPGA}$ vs. $K_{tr,WNLS}$ and of $K_{tr,nPGA}$ vs. $K_{tr,PGA}$ for the same target groups. High correlation was also observed for $K_{tr,nPGA}$ vs. $K_{tr,WNLS}$ and $K_{tr,nPGA}$ vs. $K_{tr,PGA}$ when the brain, lung and tumor ROIs were chosen as targets. The lowest correlation was observed when the muscle ROI was used as the target. Interestingly, the results for the target of tumor ROI indicated that the estimated $K_{tr,nPGA}$ were quite similar to $K_{tr,PGA}$ and $K_{tr,WNLS}$.

### 4.3. Effects of noise level in computer simulations

Table 5 lists the mean and SD for the estimated relative influx rates in the computer simulations at different noise levels. A certain pair of target and reference ROIs is specified by the subscripts in Table 5. For example, $K_{12}$ represents the relative influx rate when the brain ($t = 1$) and lung ($r = 2$) ROIs were adopted as the target and reference regions, respectively. It was observed that the mean $K_{tr,PGA}$ and mean $K_{tr,nPGA}$ both changed slightly with increasing noise levels.

The percentage biases of mean $K_{tr,PGA}$ and $K_{tr,nPGA}$ compared to $K_{tr,true}$ were also calculated. The highest bias exceeded 50% when the liver and brain ROIs were chosen as the target and reference regions, respectively. Fig. 3 plots the percentage bias of $K_{23}$ and $K_{51}$ as a function of the noise levels. It was demonstrated that the relative influx rate was insensitive to varied noise levels even when high biases were observed for the cases of liver ROI vs. brain or lung ROIs ($K_{13}$, $K_{23}$, $K_{31}$ and $K_{32}$).

Fig. 4 plots CV of the relative influx rate ($K_{54}$) as a function of the noise level, where the tumor ROI was used as the target and the muscle ROI was the reference. The reliability of $K_{54}$ for both $K_{tr,PGA}$ and $K_{tr,nPGA}$ was degraded when noise level was increasing. At the noise level of 4, the CV of $K_{tr,nPGA}$ reached about 3.5% and CV of $K_{tr,PGA}$ was about 9.4%. Similar trends of CVs were also observed for other relative influx rates by using different target and reference pairs. The CVs of most $K_{tr,PGA}$ were about as twice as those of $K_{tr,nPGA}$.

### 4.4. Effects of kinetic model in parameter estimation

For kinetic modeling, AIC and SC are usually applied in choosing the best kinetic model according to their minimum value. In the small animal studies, the four kinetic models (3c4pVb, 3c4p, 3c3pVb, and 3c3p) were used to model the FDG kinetics in brain and lung. The averages and standard deviations of AIC and SC were calculated for these four FDG kinetic models, as shown in Table 6.

For all the 15 mouse studies, the 3c4pVb model was found to have the lowest AIC and SC values for the brain in contrast to the 3c3pVb, 3c4p, and 3c3p models. Similar results were observed for the lungs: the 3c4pVb model has the lowest AIC and SC values compared with the other models. This indicated that the general FDG model is suitable to characterize the FDG kinetic in brain and lungs. The use of the general FDG model was also consistent with the previous studies in the analysis of FDG kinetics in the brain [9,15,22], and in the lungs [23].

For the muscle, the values of AIC and SC were compared between the 3c4pVb model and 5K model. Fig. 5 plots the AIC and SC values respectively for the 3c4pVb model and the 5K model across the 15 mouse studies. It was observed that similar AIC and SC values were achieved between the two models. However, much lower AIC and SC values were achieved using the 5K model for four cases while there was one case with much lower AIC and SC values using the 3c4pVb model. The performances of the 3c4pVb model and 5K model were comparable in this study. Thus, FDG kinetics in the muscle can be described by the 3c4pVb model.

In computer simulations, the four kinetic models (3c4pVb, 3c4p, 3c3pVb, and 3c3p) were used to investigate the effect of different kinetic models in estimating bias. WNLS was used to derive parameter estimates which were used as a standard for deriving the biases of the results derived by the PGA and nPGA methods. Table 7 lists the percentage bias of $K_{12}$ and $K_{52}$ estimated by PGA and nPGA method compared with the reference values for various kinetic models.

The lowest bias with the 3c3p model (≤2.0%) was achieved with both the PGA and nPGA methods. The introduction of $k_4$ in the 3c4p model led to the bias with the increase of about 10% for PGA and 6% for nPGA. Comparing the 3c3p and 3c3pVb models shows that the introduction of vascular volume also resulted in at least 7% increase in the bias for PGA and nPGA method. No significant increase of bias was observed for nPGA between the 3c3pVb and 3c4pVb models.

## 5. Discussion

The FDG dynamic behaviour in liver is complex and specific. It has been proposed to use a dual blood input in describing tracer kinetics of liver [24,25]. However, it is impractical to delineate ROIs of the dual blood vessels of the liver in small animal studies due to the small blood vessels of the subjects and the limited spatial resolution of the scanner. Thus, the assumption of one blood input function was inherited from the previous small-animal studies [9,22], and the general FDG kinetic model was used for the liver in this paper. Overall, it was reasonable to apply the general FDG model in the simulation and WNLS fitting because the focus of this paper was to evaluate the performance of nPGA through the comparisons with traditional PGA in whole-body mouse studies, in order to address the challenging issue of invasive blood sampling in small animal studies. The use of the general FDG model provides a simple and practical approach, consistent with previous mouse studies in the literature [8,9,22].

From the results of the small animal studies and computer simulations, it can be determined that the nPGA method was not efficient when the liver was used as either the reference ROI or the target ROI. The PGA method was originally proposed for the simplified FDG model with one irreversible compartment for FDG-6-$PO_4$ in tissue ($k_4 = 0$). Since the nPGA method is based upon the PGA method, nPGA should be efficient for tissues with a low value of $k_4$. If $k_4$ is sufficiently lower than the other rate constants, the tracer can be assumed to be irreversibly trapped and $k_4$ can be neglected. However, this assumption of tracer kinetics is violated in the liver. The results of the estimated rate constants in Table 1 show that for the liver the average $k_4$ was comparable with $k_3$, whereas in the brain, where nPGA and PGA methods performed better, the average $k_4$ was approximately 10% of $k_3$. Since the PGA and nPGA methods both rely on the simplified FDG model, which is different from the general FDG model, the effects of the $k_4$ and vascular effects on estimated biases were investigated in this paper. The results demonstrated that more estimated biases were observed in the PGA method than the nPGA method when $k_4$ or the vascular effects were included in the kinetic model. This may imply that the procedure for the estimation of the relative influx rate in the nPGA method somehow compensates for the bias during the calculation of the influx rates of the individual ROIs using the PGA method. The results of the Bland–Altman plots in Fig. 2 demonstrated that most of all percent differences are within the range of limits of agreement both for $K_{tr,nPGA}$ vs. $K_{tr,WNLS}$ and $K_{tr,nPGA}$ vs. $K_{tr,PGA}$. This indicates that nPGA, PGA and WNLS methods can be used interchangeably to derive the estimates of the relative influx rates, while the agreement of $K_{tr,nPGA}$ vs. $K_{tr,PGA}$ is better than that of $K_{tr,nPGA}$ vs. $K_{tr,WNLS}$. The result coincides with the assumption of nPGA method.

The computer simulations were performed with varied noise levels added for evaluating the effects of noise on the PGA and nPGA methods. The fact that the average $K_{tr,PGA}$ and $K_{tr,WNLS}$ changed very slightly with increasing noise level demonstrated that the relative influx rate was insensitive to noise levels. Moreover, the results of the CVs indicated that the reliability of $K_{tr,PGA}$ became worse than that of $K_{tr,nPGA}$ with increasing noise levels. This may imply that the use of a reference ROI somehow reduces the effect of noise in the generation of the relative influx rate of the target ROI.

When the target ROI was placed on the tumor in computer simulations, the accuracy of the relative influx rate achieved by the nPGA method was considerably higher than that obtained by the PGA method. A high linear correlation was also achieved between $K_{tr,nPGA}$ vs. $K_{tr,WNLS}$ and $K_{tr,nPGA}$ vs. $K_{tr,PGA}$ for the tumor target in small animal studies. The relative influx rates derived by the nPGA method were reasonably close to the values of $K_{tr,WNLS}$ compared to those obtained via the PGA method in small animal studies. This implies that the nPGA method may be superior in the non-invasive quantification of tumors when a suitable reference is available. Because the nPGA method is based upon the PGA method, a suitable reference could be a tissue with low $k_4$ in the general FDG kinetic model, where the tracer can be assumed to be irreversibly trapped. The results of the small animal studies show that the values of $k_4$ for the brain and lungs were relatively lower. Moreover, the results showed that the brain and lungs could be used as suitable references for the derivation of acceptable relative influx rates by the nPGA method. If the tracer kinetics of the target and reference regions are very distinct, the nPGA method would have a better performance. This may be the reason that the good results are obtained for the tumor target, where the FDG kinetics is very different from other regions.

The range of data used in the PGA method may affect the estimates of the slope in the linear plot. This causes a slight instability in the PGA method. In previous studies, the range of the data has been recommended as 3–22 min in order to minimize the effect of $k_4$ [15,22]. The range of data used in the PGA method was adopted in order to obtain the target influx rates for ROIs of the selected major organs. The optimal range of the data used in nPGA cannot be derived from the processes which deduce the nPGA method. Thus, a range of $t > 3$ min was used in the nPGA method presented in this paper. The PGA method is often compared with the use of the standard uptake value (SUV), a popular semi-quantitative index for the analysis of PET images in cancer diagnosis [26,27]. A comparison between the SUV and nPGA methods will be investigated in the future studies as well as the investigation in non-invasive tumor quantification of human by using nPGA method.

## 6. Conclusion

The performance of the nPGA method was systematically investigated by 15 whole-body FDG-PET studies of mice and computer simulations. The mouse studies showed high linearity of relative influx rates between the nPGA and PGA for most reference and target pairs, when an appropriate underlying kinetic model was used. The results of computer simulations demonstrated that the accuracy of the nPGA method was similar to that of the PGA method, with a higher reliability for most reference and target pairs. In particular, nPGA method could be recommended as a non-invasive and indirect method for the quantification of MRGlc in tumor in small animal studies.

## Acknowledgments

The authors would like to thank David Truong, David Vu and Weber Shao at the Department of Molecular & Medical Pharmacology, UCLA for their IT support and the staff at the Crump Institute for Molecular Imaging for their technical assistance in small animal imaging. This research was partially supported by China Postdoctoral Science Foundation, Hong Kong PolyU grants and ARC grants.

## Appendix

The nPGA method is based upon the PGA method, with the assumption that the whole-body is a SIMO system. For the PGA method, the FDG concentration can be expressed as a relationship with the PTAC as given in (A1).

$$C_t(t)=K_i\int_0^t C_p(\tau)d\tau+IC_p(t),\ t>t^* \tag{A1}$$

The TTACs of two distinct ROIs (one being the reference ROI, the other being the target ROI) can be described by (A2).

$$\begin{cases} C_{ref}(t)=K_{ref}\int_0^t C_p(\tau)d\tau+I_{ref}C_p(t) \\ C_{tg}(t)=K_{tg}\int_0^t C_p(\tau)d\tau+I_{tg}C_p(t) \end{cases},\ t>t^* \tag{A2}$$

According to (A2), the PTAC can be presented by (A3).

$$\begin{cases} \int_0^t C_p(\tau)d\tau=\frac{I_{tg}C_{ref}(t)-I_{ref}C_{tg}(t)}{D} \\ C_p(t)=\frac{-K_{tg}C_{ref}(t)+K_{ref}C_{tg}(t)}{D} \end{cases},\ D=K_{ref}I_{tg}-K_{tg}I_{ref},\ t>t^* \tag{A3}$$

(A4) is obtained by integrating both sides of the second equation in (A3).

$$\int_{t_0}^t C_p(\tau)d\tau=\int_{t_0}^t\frac{[-K_{tg}C_{ref}(\tau)+K_{ref}C_{tg}(\tau)]}{D}d\tau=\frac{-K_{tg}\int_{t_0}^t C_{ref}(\tau)d\tau+K_{ref}\int_{t_0}^t C_{tg}(\tau)d\tau}{D} \tag{A4}$$

Because

$\int_0^t C_p(\tau)d\tau=\int_0^{t_0} C_p(\tau)d\tau+\int_{t_0}^t C_p(\tau)d\tau,\ t>t_0>t^*$ and $\int_0^{t_0} C_p(\tau)d\tau=\frac{I_{tg}C_{ref}(t_0)-I_{ref}C_{tg}(t_0)}{D}$, (A5) can be obtained from (A3) and (A4).

$$\frac{I_{tg}C_{ref}(t)-I_{ref}C_{tg}(t)}{D}=\frac{I_{tg}C_{ref}(t_0)-I_{ref}C_{tg}(t_0)}{D}+\frac{-K_{tg}\int_{t_0}^t C_{ref}(\tau)d\tau+K_{ref}\int_{t_0}^t C_{tg}(\tau)d\tau}{D} \tag{A5}$$

To eliminate $D$ in (A5), a new equation expressing the relationship between two TTACs, is given by (A6).

$$K_{ref}\int_{t_0}^t C_{tg}(\tau)d\tau=K_{tg}\int_{t_0}^t C_{ref}(\tau)d\tau+I_{tg}[C_{ref}(t)-C_{ref}(t_0)]-I_{ref}[C_{tg}(t)-C_{tg}(t_0)] \tag{A6}$$

Finally, the nPGA method can be presented by the equation in (A7). The relative influx rate can then be derived by liner least squares method.

$$\begin{aligned}\int_{t_0}^{t} C_{tg}(\tau)d\tau &= \frac{K_{tg}}{K_{ref}}\int_{t_0}^{t} C_{ref}(\tau)d\tau \\ &+ \frac{I_{tg}}{K_{ref}}[C_{ref}(t) \\ &- C_{ref}(t_0)] \\ &- \frac{I_{ref}}{K_{ref}}[C_{tg}(t) \\ &- C_{tg}(t_0)] = K_{tr}\int_{t_0}^{t} C_{ref}(\tau)d\tau + I_{tr}[C_{ref}(t) \\ &- C_{ref}(t_0)] \\ &- I_{rr}[C_{tg}(t) \\ &- C_{tg}(t_0)], \\ t > t_0 > t^*\end{aligned} \tag{A7}$$

## References


1. Gambhir SS, et al. A tabulated summary of the FDG PET literature. J. Nucl. Med. 2001 May 1.42:1S–93S. [PubMed: 11483694]
2. Feng, DD., et al. Techniques for parametric imaging. In: Feng, DD., editor. Biomedical Information Technology. Elsevier; 2008. p. 137-159.
3. Gambhir, SS. Quantitative assay development for PET. In: Phelps, ME., editor. PET: Molecular Imaging and Its Biological Applications. Springer-Verlag; 2004. p. 125-216.
4. Patlak CS, Blasberg RG. Graphical evaluation of blood-to-brain transfer constants from multiple-time uptake data. Generalizations. J. Cereb. Blood Flow Metab. 1985 Dec.5:584–590. [PubMed: 4055928]
5. Logan J, et al. Graphical analysis of reversible radioligand binding from time–activity measurements applied to [N-11C-methyl]-(−)-cocaine PET studies in human subjects. J. Cereb. Blood Flow Metab. 1990 Sep.10:740–747. [PubMed: 2384545]
6. Lin KP, et al. Correction of spillover radioactivities for estimation of the blood time–activity curve from the imaged LV chamber in cardiac dynamic FDG PET studies. Phys. Med. Biol. 1995 Apr. 40:629–642. [PubMed: 7610118]
7. Feng D, et al. A new double modeling approach for dynamic cardiac PET studies using noise and spillover contaminated LV measurements. IEEE Trans. Biomed. Eng. 1996; 43:319–327. [PubMed: 8682545]
8. Fang Y-HD, Muzic RF Jr. Spillover and partial-volume correction for image-derived input functions for small-animal 18F-FDG PET studies. J. Nucl. Med. 2008 Apr 1.49:606–614. [PubMed: 18344438]
9. Ferl GZ, et al. Estimation of the $^{18}$F-FDG input function in mice by use of dynamic small-animal PET and minimal blood sample data. J. Nucl. Med. 2007 Dec 1.48:2037–2045. [PubMed: 18006615]
10. Eidelberg D, et al. Positron emission tomographic findings in Filipino X-linked dystonia-parkinsonism. Ann. Neurol. 1993 Aug.34:185–191. [PubMed: 8338342]
11. Eberl S, et al. Evaluation of two population-based input functions for quantitative neurological FDG PET studies. Eur. J. Nucl. Med. 1997 Mar.24:299–304. [PubMed: 9143468]
12. Feng D, et al. A technique for extracting physiological parameters and the required input function simultaneously from PET image measurements: theory and simulation study. IEEE Trans. Inf. Technol. Biomed. 1997 Dec.1:243–254. [PubMed: 11020827]

13. Logan J, et al. Distribution volume ratios without blood sampling from graphical analysis of PET data. J. Cereb. Blood Flow Metab. 1996; 16:834–840. [PubMed: 8784228]
14. Wu Y-G. Noninvasive quantification of local cerebral metabolic rate of glucose for clinical application using positron emission tomography and F-fluoro-2-deoxy-d-glucose. J. Cereb. Blood Flow Metab. 2007; 28:242–250. [PubMed: 17684521]
15. Wu H-M, et al. In vivo quantitation of glucose metabolism in mice using small-animal PET and a microfluidic device. J. Nucl. Med. 2007 May.48:837–845. [PubMed: 17475972]
16. Loening AM, Gambhir SS. AMIDE: a free software tool for multimodality medical image analysis. Mol. Imaging. 2003 Jul.2:131–137. [PubMed: 14649056]
17. Chen KW, et al. The effects of measurement errors in the plasma radioactivity curve on parameter estimation in positron emission tomography. Phys. Med. Biol. 1991 Sep.36:1183–1200. [PubMed: 1946602]
18. Logan J, et al. A strategy for removing the bias in the graphical analysis method. J. Cereb. Blood Flow Metab. 2001 Mar.21:307–320. [PubMed: 11295885]
19. Huang SC, et al. An internet-based “kinetic imaging system” (KIS) for MicroPET. Mol. Imaging Biol. 2005 Sep-Oct;7:330–341. [PubMed: 16132473]
20. Bertoldo A, et al. Kinetic modeling of [18F]FDG in skeletal muscle by PET: a four-compartment five-rate-constant model. Am. J. Physiol. Endocrinol. Metab. 2001 Sep 1.281:E524–E536. [PubMed: 11500308]
21. Stone M. Comments on model selection criteria of akaike and schwarz. J. Roy. Stat. Soc. Ser. B (Methodol.). 1979; 41:276–278.
22. Yu AS, et al. Quantification of cerebral glucose metabolic rate in mice using 18F-FDG and small-animal PET. J. Nucl. Med. 2009 Jun 1.50:966–973. [PubMed: 19443595]
23. Chen DL, et al. Comparison of methods to quantitate $^{18}$F-FDG uptake with PET during experimental acute lung injury. J. Nucl. Med. 2004 Sep 1.45:1583–1590. [PubMed: 15347728]
24. Chen S, Feng D. Noninvasive quantification of the differential portal and arterial contribution to the liver blood supply from PET measurements using the $^{11}$C-acetate kinetic model. IEEE Trans. Biomed. Eng. 2004; 51:1579–1585. [PubMed: 15376506]
25. Munk OL, et al. Liver kinetics of glucose analogs measured in pigs by PET: importance of dual-input blood sampling. J. Nucl. Med. 2001 May.42:795–801. [PubMed: 11337579]
26. Wu H, et al. Quantitative evaluation of skeletal tumours with dynamic FDG PET: SUV in comparison to Patlak analysis. Eur. J. Nucl. Med. 2001 Jun.28:704–710. [PubMed: 11440030]
27. Freedman NM, et al. Comparison of SUV and Patlak slope for monitoring of cancer therapy using serial PET scans. Eur. J. Nucl. Med. 2003 Jun.30:46–53.

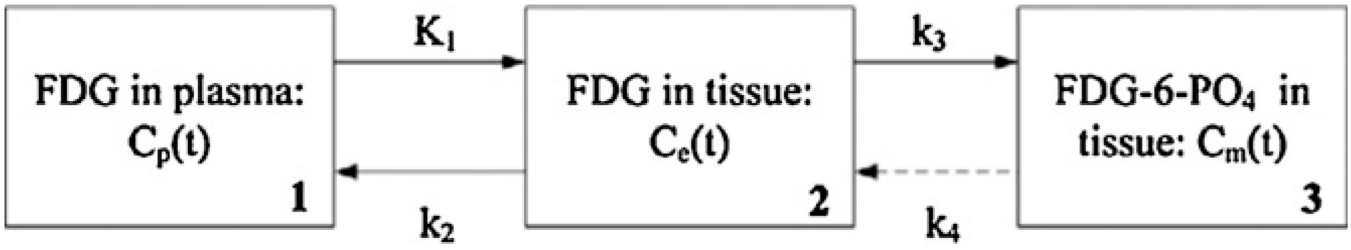


**Fig. 1.**

The three-compartment and four-parameter model of FDG. $K_1$, $k_2$, $k_3$, and $k_4$ are the rate constants between the compartments; compartment 1 and 2 are for FDG in plasma and tissue, respectively, while compartment 3 is for the phosphorated FDG (FDG-6-$PO_4$) in tissue; $k_4$ can be neglected in some cases (depicted with a dotted line).

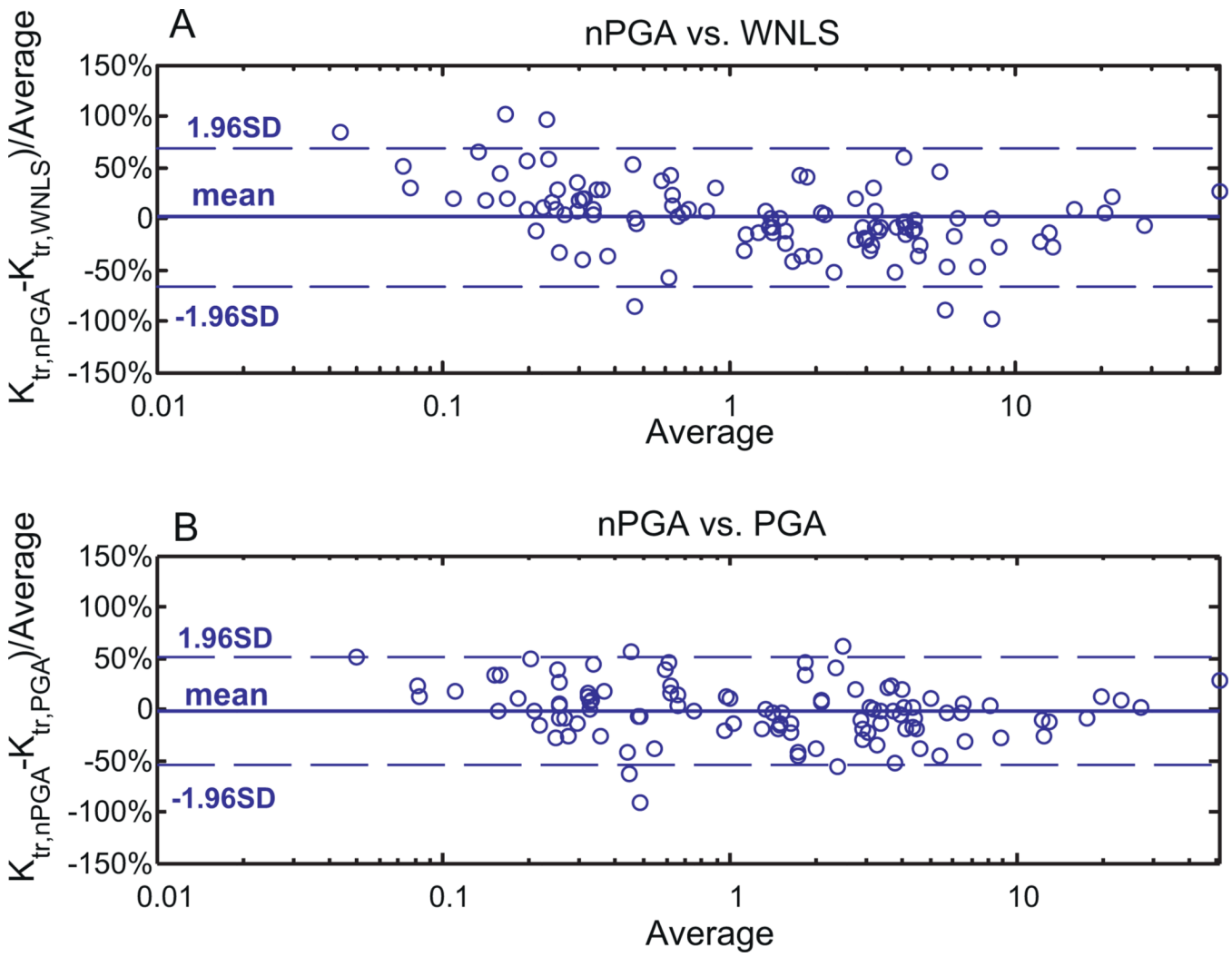


**Fig. 2.**

The agreements of relative influx rates estimated by different methods using the Bland–Altman plot. (A) $K_{tr,nPGA}$ and $K_{tr,WNLS}$; (B) $K_{tr,nPGA}$ and $K_{tr,PGA}$. Each subfigure displays a scatter diagram of the differences plotted against the averages of the two estimates. Horizontal lines are drawn at the mean difference (bold solid line), and at the limits of agreement, which are defined as the mean difference plus and minus 1.96 times the standard deviation of the differences (dash lines).

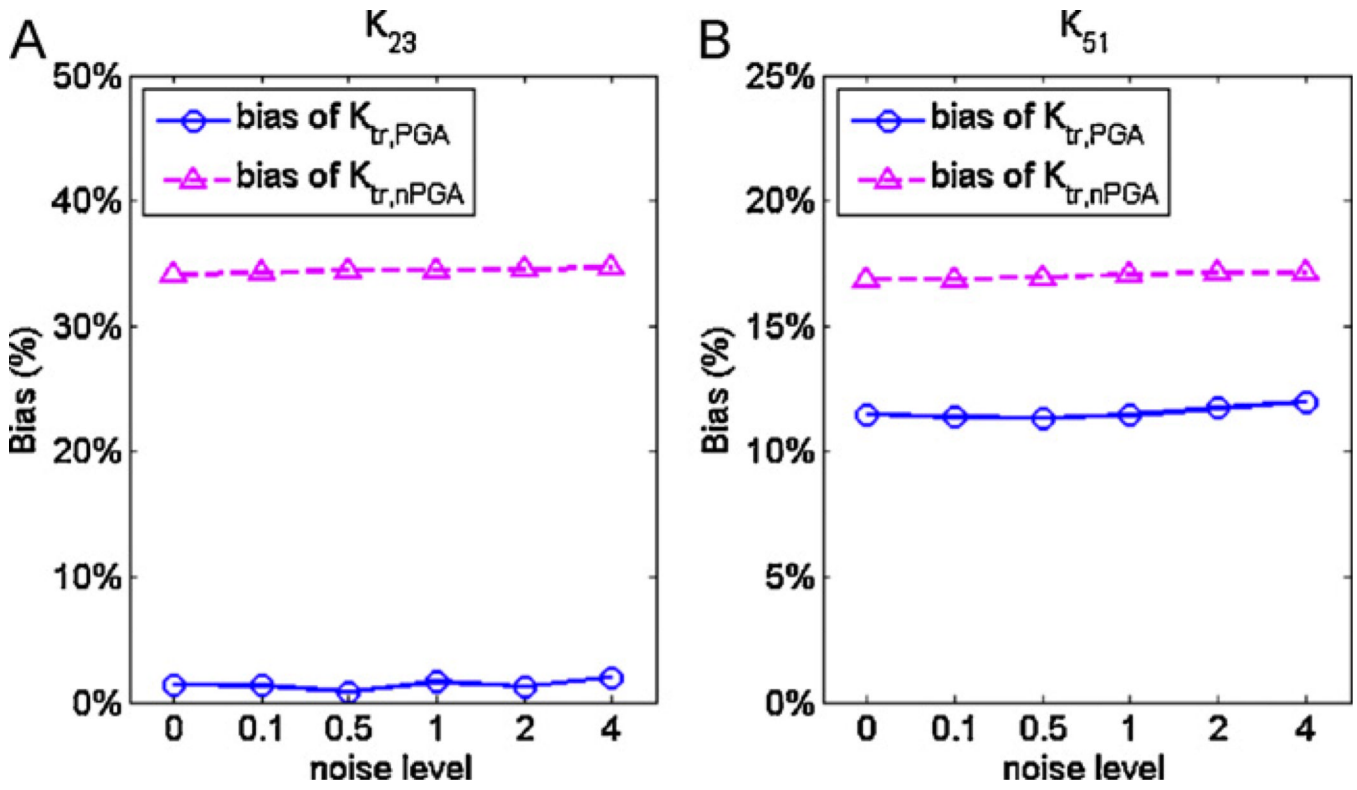


**Fig. 3.**

Plots of the percentage bias at different noise levels, for the relative influx rates: (A) $K_{23}$ and (B) $K_{51}$, as estimated by both PGA and nPGA.

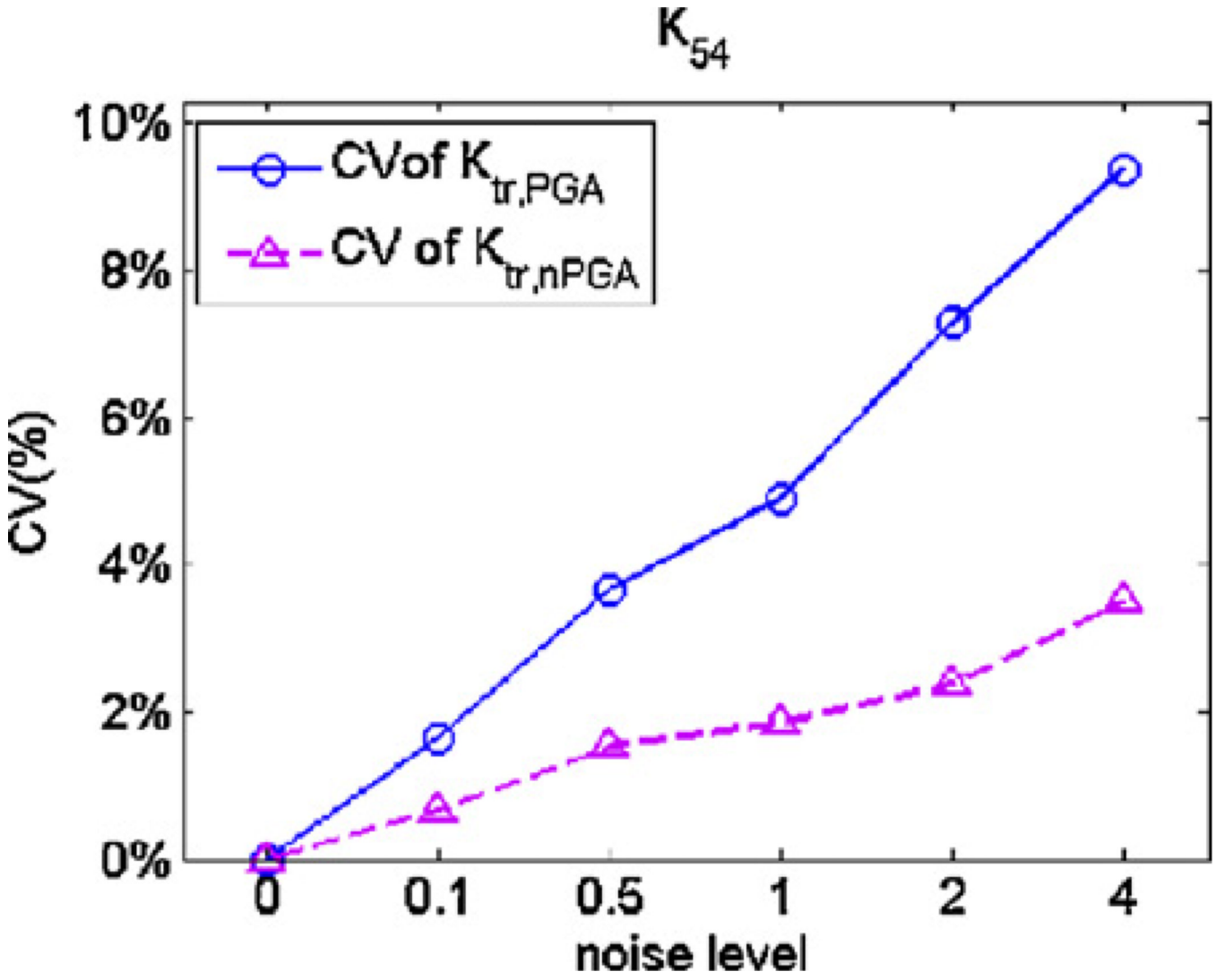


**Fig. 4.**
Coefficient variations (CV) of the relative influx rate ($K_{54}$) estimated by the PGA and nPGA methods at different noise levels.

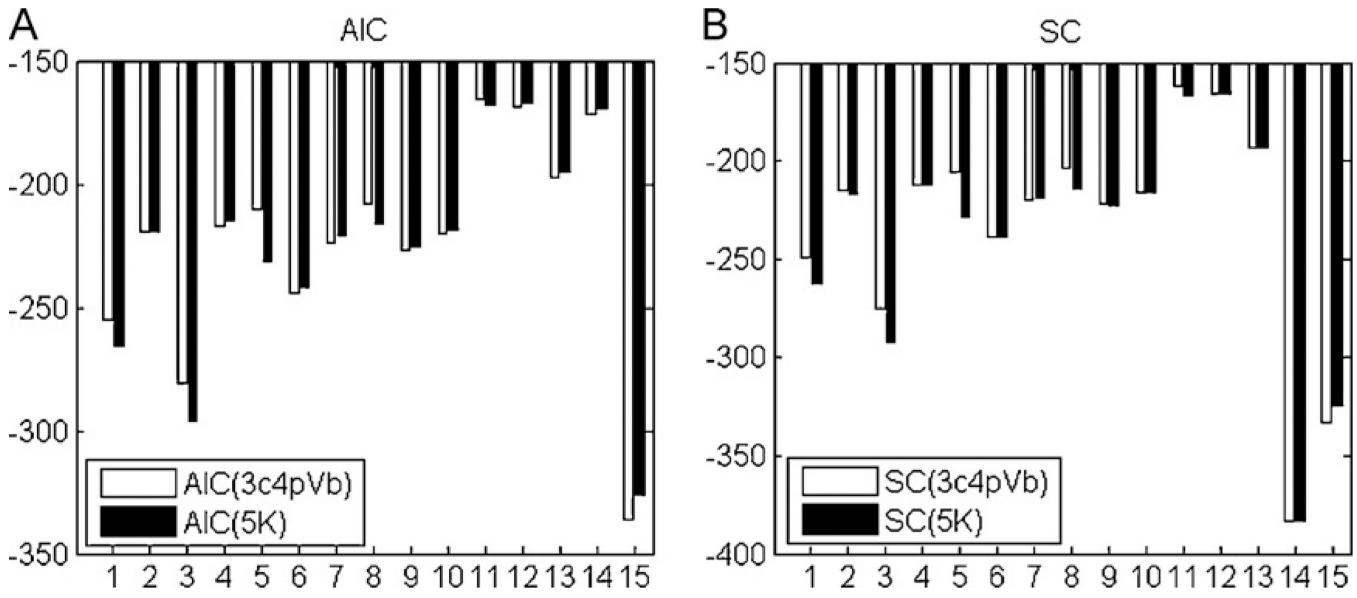


**Fig. 5.**

Comparisons between the general FDG kinetic model and 5K model in fitting TTACs of muscle: (A) AIC values; (B) SC values.

**Table 1**

The obtained rate constants (mean ± SD) for 15 FDG-PET studies of mice.

| **ROI #** | **1** | **2** | **3** | **4** | **5** |
|---|---|---|---|---|---|
| Parameter | Brain | Lung | Liver | Muscle | Tumor[a] |
| $K_1$ (ml min$^{-1}$ ml$^{-1}$) | 0.217 ± 0.131 | 0.139 ± 0.091 | 0.840 ± 0.381 | 0.036 ± 0.019 | 0.221 ± 0.076 |
| $k_2$ (min$^{-1}$) | 0.413 ± 0.127 | 0.644 ± 0.366 | 1.432 ± 0.679 | 0.324 ± 0.148 | 0.263 ± 0.243 |
| $k_3$ (min$^{-1}$) | 0.113 ± 0.090 | 0.104 ± 0.029 | 0.020 ± 0.013 | 0.074 ± 0.088 | 0.712 ± 0.359 |
| $k_4$ (min$^{-1}$) | 0.017 ± 0.005 | 0.011 ± 0.006 | 0.009 ± 0.008 | 0.019 ± 0.023 | 0.021 ± 0.014 |
| $V_b$ (ml ml$^{-1}$) | 0.076 ± 0.046 | 0.161 ± 0.061 | 0.098 ± 0.085 | 0.014 ± 0.010 | 0.057 ± 0.034 |

[a]The results with tumor as target are derived from the five studies of tumor-bearing mice.

*Biomed Signal Process Control*. Author manuscript; available in PMC 2012 September 04.

**Table 2**

Relative influx rates (mean ± SD) in small animal studies.

| Reference | $K_{tr}$ | Target | | | | |
|---|---|---|---|---|---|---|
| | | 1 brain | 2 lung | 3 liver | 4 muscle | 5 tumor[a] |
| 1 brain | $K_{tr,WNLS}$ | | 0.55 ± 0.27 | 0.37 ± 0.27 | 0.17 ± 0.11 | 1.58 ± 0.43 |
| | $K_{tr,PGA}$ | | 0.55 ± 0.26 | 0.24 ± 0.26 | 0.20 ± 0.11 | 1.69 ± 0.40 |
| | $K_{tr,nPGA}$ | | 0.62 ± 0.24 | 0.57 ± 0.29 | 0.19 ± 0.09 | 1.76 ± 0.44 |
| 2 lung | $K_{tr,WNLS}$ | 2.25 ± 1.05 | | 0.64 ± 0.22 | 0.32 ± 0.19 | 5.07 ± 0.84 |
| | $K_{tr,PGA}$ | 2.21 ± 0.96 | | 0.44 ± 0.14 | 0.37 ± 0.18 | 5.23 ± 0.81 |
| | $K_{tr,nPGA}$ | 1.85 ± 0.83 | | 0.86 ± 0.26 | 0.31 ± 0.10 | 5.14 ± 1.06 |
| 3 liver | $K_{tr,WNLS}$ | 4.04 ± 2.45 | 1.72 ± 0.51 | | 0.53 ± 0.30 | 10.53 ± 1.06 |
| | $K_{tr,PGA}$ | 5.72 ± 3.10 | 2.61 ± 1.12 | | 0.95 ± 0.63 | 13.81 ± 4.15 |
| | $K_{tr,nPGA}$ | 2.35 ± 1.53 | 1.24 ± 0.39 | | 0.35 ± 0.14 | 8.68 ± 1.88 |
| 4 muscle | $K_{tr,WNLS}$ | 9.89 ± 9.44 | 4.25 ± 2.61 | 2.6 ± 1.60 | | 27.13 ± 19.26 |
| | $K_{tr,PGA}$ | 7.96 ± 6.37 | 3.37 ± 1.70 | 1.46 ± 0.92 | | 23.39 ± 11.69 |
| | $K_{tr,nPGA}$ | 7.10 ± 6.23 | 3.58 ± 1.55 | 3.22 ± 1.59 | | 26.15 ± 18.49 |

[a]The results with the tumor as the target are derived from five studies of tumor-bearing mice.

*Biomed Signal Process Control*. Author manuscript; available in PMC 2012 September 04.

**Table 3**

A summary of linear regression analysis for the same reference groups.

| Reference ($y = ax + b$) | $K_{tr,nPGA}$ vs. $K_{tr,WNLS}$ | | | $K_{tr,nPGA}$ vs. $K_{tr,PGA}$ | | |
|---|---|---|---|---|---|---|
| | $a$ | $b$ | $R^2$ | $a$ | $b$ | $R^2$ |
| Brain | 1.01 | 0.102 | 0.953 | 0.944 | 0.151 | 0.923 |
| Lung | 0.918 | 0.0702 | 0.971 | 0.891 | 0.146 | 0.964 |
| Liver | 0.764 | −0.197 | 0.959 | 0.525 | −0.134 | 0.884 |
| Muscle | 1.105 | −0.635 | 0.915 | 1.122 | −0.036 | 0.939 |

**Table 4**

A summary of linear regression for the same target groups.

| Target ($y = ax + b$) | $K_{tr,nPGA}$ vs. $K_{tr,WNLS}$ | | | $K_{tr,nPGA}$ vs. $K_{tr,PGA}$ | | |
|---|---|---|---|---|---|---|
| | $a$ | $b$ | $R^2$ | $a$ | $b$ | $R^2$ |
| Brain | 0.663 | 0.185 | 0.979 | 0.824 | −0.455 | 0.894 |
| Lung | 0.673 | 0.321 | 0.918 | 0.754 | 0.161 | 0.812 |
| Liver | 1.05 | 0.257 | 0.941 | 1.76 | 0.264 | 0.874 |
| Muscle | 0.480 | 0.114 | 0.708 | 0.174 | 0.194 | 0.317 |
| Tumor[a] | 0.955 | −0.155 | 0.994 | 1.18 | −2.58 | 0.945 |

[a]The results with the tumor ROI as the target are derived from five studies of tumor-bearing mice.

*Biomed Signal Process Control*. Author manuscript; available in PMC 2012 September 04.

**Table 5**

Relative influx rates ($K_{tr}$) (mean ± SD) at various noise levels.

| **Ref.** | **Brain** | | | | **Lung** | | | | **Liver** | | | | **Muscle** | | | |
|---|---|---|---|---|---|---|---|---|---|---|---|---|---|---|---|---|
| **Target** | **Lung** | **Liver** | **Muscle** | **Tumor** | **Brain** | **Liver** | **Muscle** | **Tumor** | **Brain** | **Lung** | **Muscle** | **Tumor** | **Brain** | **Lung** | **Liver** | **Tumor** |
| $K_{tr}$ | $K_{21}$ | $K_{31}$ | $K_{41}$ | $K_{51}$ | $K_{12}$ | $K_{32}$ | $K_{42}$ | $K_{52}$ | $K_{13}$ | $K_{23}$ | $K_{43}$ | $K_{53}$ | $K_{14}$ | $K_{24}$ | $K_{34}$ | $K_{54}$ |
| $K_{\text{tr,ture}}$ | 0.41 | 0.25 | 0.12 | 3.46 | 2.41 | 0.60 | 0.28 | 8.35 | 4.03 | 1.67 | 0.47 | 13.95 | 8.49 | 3.52 | 2.11 | 29.41 |
| *(a) 1 run with noise level c = 0 (noise free)* | | | | | | | | | | | | | | | | |
| $K_{\text{tr,PGA}}$ | 0.38 | 0.23 | 0.14 | 3.86 | 2.60 | 0.61 | 0.37 | 10.03 | 4.28 | 1.65 | 0.61 | 16.52 | 7.08 | 2.72 | 1.65 | 27.31 |
| $K_{\text{tr,nPGA}}$ | 0.44 | 0.41 | 0.15 | 4.05 | 2.26 | 0.92 | 0.34 | 9.49 | 2.43 | 1.10 | 0.38 | 11.85 | 6.64 | 2.91 | 2.63 | 27.73 |
| *(b) 100 runs with noise level c = 0.1* | | | | | | | | | | | | | | | | |
| $K_{\text{tr,PGA}}$ | 0.38 ± 0.0040 | 0.23 ± 0.0044 | 0.14 ± 0.0024 | 3.86 ± 0.023 | 2.61 ± 0.027 | 0.61 ± 0.013 | 0.37 ± 0.0068 | 10.05 ± 0.093 | 4.30 ± 0.082 | 1.65 ± 0.034 | 0.61 ± 0.015 | 16.56 ± 0.304 | 7.08 ± 0.123 | 2.72 ± 0.050 | 1.65 ± 0.041 | 27.31 ± 0.448 |
| $K_{\text{tr,nPGA}}$ | 0.44 ± 0.0013 | 0.41 ± 0.0027 | 0.15 ± 0.0010 | 4.05 ± 0.012 | 2.26 ± 0.0066 | 0.91 ± 0.0071 | 0.34 ± 0.0018 | 9.49 ± 0.041 | 2.43 ± 0.016 | 1.10 ± 0.010 | 0.38 ± 0.002 | 11.84 ± 0.130 | 6.63 ± 0.050 | 2.90 ± 0.015 | 2.63 ± 0.012 | 27.65 ± 0.182 |
| *(c) 100 runs with noise level c = 0.5* | | | | | | | | | | | | | | | | |
| $K_{\text{tr,PGA}}$ | 0.38 ± 0.0093 | 0.23 ± 0.010 | 0.14 ± 0.0054 | 3.85 ± 0.047 | 2.61 ± 0.064 | 0.60 ± 0.028 | 0.37 ± 0.015 | 10.07 ± 0.231 | 4.33 ± 0.181 | 1.66 ± 0.077 | 0.61 ± 0.034 | 16.68 ± 0.684 | 7.12 ± 0.270 | 2.73 ± 0.115 | 1.65 ± 0.089 | 27.43 ± 1.00 |
| $K_{\text{tr,nPGA}}$ | 0.44 ± 0.0013 | 0.41 ± 0.0034 | 0.15 ± 0.0023 | 4.05 ± 0.027 | 2.25 ± 0.013 | 0.91 ± 0.012 | 0.34 ± 0.004 | 9.47 ± 0.081 | 2.45 ± 0.020 | 1.10 ± 0.014 | 0.38 ± 0.004 | 11.71 ± 0.238 | 6.56 ± 0.108 | 2.89 ± 0.036 | 2.63 ± 0.026 | 27.69 ± 0.424 |
| *(d) 100 runs with noise level c = 1.0* | | | | | | | | | | | | | | | | |
| $K_{\text{tr,PGA}}$ | 0.38 ± 0.013 | 0.23 ± 0.014 | 0.14 ± 0.0075 | 3.86 ± 0.070 | 2.60 ± 0.087 | 0.61 ± 0.039 | 0.37 ± 0.020 | 10.04 ± 0.34 | 4.27 ± 0.246 | 1.64 ± 0.104 | 0.60 ± 0.045 | 16.47 ± 0.901 | 7.12 ± 0.379 | 2.74 ± 0.145 | 1.67 ± 0.124 | 27.44 ± 1.34 |
| $K_{\text{tr,nPGA}}$ | 0.44 ± 0.0037 | 0.41 ± 0.0040 | 0.15 ± 0.0035 | 4.05 ± 0.042 | 2.25 ± 0.019 | 0.91 ± 0.012 | 0.34 ± 0.004 | 9.46 ± 0.108 | 2.45 ± 0.024 | 1.10 ± 0.015 | 0.38 ± 0.005 | 11.65 ± 0.319 | 6.51 ± 0.162 | 2.89 ± 0.037 | 2.63 ± 0.035 | 27.80 ± 0.515 |
| *(e) 100 runs with noise level c = 2.0* | | | | | | | | | | | | | | | | |
| $K_{\text{tr,PGA}}$ | 0.38 ± 0.018 | 0.23 ± 0.018 | 0.14 ± 0.0099 | 3.87 ± 0.102 | 2.62 ± 0.124 | 0.61 ± 0.054 | 0.37 ± 0.028 | 10.12 ± 0.413 | 4.31 ± 0.349 | 1.65 ± 0.149 | 0.61 ± 0.060 | 16.67 ± 1.34 | 7.13 ± 0.513 | 2.73 ± 0.213 | 1.66 ± 0.162 | 27.56 ± 2.01 |
| $K_{\text{tr,nPGA}}$ | 0.44 ± 0.0053 | 0.41 ± 0.0055 | 0.16 ± 0.0051 | 4.05 ± 0.058 | 2.25 ± 0.027 | 0.91 ± 0.015 | 0.35 ± 0.0070 | 9.42 ± 0.157 | 2.46 ± 0.034 | 1.09 ± 0.019 | 0.38 ± 0.007 | 11.43 ± 0.419 | 6.41 ± 0.217 | 2.86 ± 0.058 | 2.63 ± 0.049 | 27.65 ± 0.658 |
| *(f) 100 runs with noise level c = 4.0* | | | | | | | | | | | | | | | | |
| $K_{\text{tr,PGA}}$ | 0.39 ± 0.025 | 0.23 ± 0.029 | 0.14 ± 0.014 | 3.88 ± 0.137 | 2.60 ± 0.165 | 0.60 ± 0.080 | 0.37 ± 0.045 | 10.06 ± 0.648 | 4.41 ± 0.589 | 1.70 ± 0.241 | 0.62 ± 0.092 | 17.07 ± 2.17 | 7.13 ± 0.680 | 2.76 ± 0.328 | 1.64 ± 0.233 | 27.60 ± 2.59 |
| $K_{\text{tr,nPGA}}$ | 0.44 ± 0.0072 | 0.41 ± 0.0085 | 0.16 ± 0.0067 | 4.05 ± 0.067 | 2.25 ± 0.036 | 0.92 ± 0.021 | 0.35 ± 0.010 | 9.41 ± 0.277 | 2.46 ± 0.053 | 1.09 ± 0.025 | 0.38 ± 0.012 | 11.26 ± 0.531 | 6.33 ± 0.277 | 2.85 ± 0.076 | 2.63 ± 0.080 | 27.84 ± 0.978 |

**Table 6**

AIC and SC (mean ± SD) of different kinetic models for brain and lung.

| Kinetic model | brain | | lung | |
|---|---|---|---|---|
| | AIC | SC | AIC | SC |
| 3c4pVb | −307.8 ± 44.1 | −300.3 ± 44.1 | −304.8 ± 45.7 | −297.3 ± 45.7 |
| 3c4p | −275.6 ± 50 | −269.6 ± 50 | −246.9 ± 39.5 | −240.9 ± 39.5 |
| 3c3pVb | −270.5 ± 41.4 | −264.5 ± 41.4 | −259.2 ± 30.4 | −253.2 ± 30.4 |
| 3c3p | −245.3 ± 36.2 | −240.8 ± 36.2 | −235.8 ± 31.2 | −231.3 ± 31.3 |

**Table 7**

Percentage bias of $K_{12}$ and $K_{52}$ derived by PGA and nPGA methods compared with reference values for different models at noise level $c = 0$.

| | **Bias** | **3c4pVb** | **3c4p** | **3c3pVb** | **3c3p** |
|---|---|---|---|---|---|
| $K_{12}$ | PGA | 7.9% | 11.6% | 7.5% | 2.0% |
| | nPGA | 6.4% | 6.1% | 15.9% | 1.2% |
| $K_{52}$ | PGA | 30.7% | 16.3% | 23.5% | 0.9% |
| | nPGA | 13.6% | 6.0% | 11.6% | 0.03% |

*Biomed Signal Process Control*. Author manuscript; available in PMC 2012 September 04.